DIAGNOSTYKA, 2024, Vol. 25, No. 2

MECHANICAL BEHAVIOR AND FAILURE MECHANISM OF RESISTANCE SPOT WELDED ALUMINUM AND COPPER JOINT USED IN THE LIGHTWEIGHT STRUCTURES

Marwah Sabah FAKHRI [1, 2 *] ⓘ **, Ahmed AL-MUKHTAR** [3, 4] ⓘ **, Ibtihal A. MAHMOOD** [2] ⓘ

[1] Ministry of Higher Education and Scientific Research, Baghdad, Iraq
[2] University of Technology-Iraq, Mechanical Engineering Department, Baghdad, Iraq
[3] College of Engineering, Al-Hussain University College, Iraq
[4] Institute of Structural Mechanics, Bauhaus-Universität Weimar, Germany
[*] Corresponding author email: me.20.24@grad.uotechnology.edu.iq

Abstract

Recently, dissimilar metals have found applications in the process of resistance spot welding (RSW), particularly within the electric vehicle industry. Notably, copper and aluminum have gained significant importance in these sectors due to their advantageous characteristics for the industry requirements. The mechanical behavior of these materials is essential to maintaining structural integrity. The study aims to estimate the mechanical behavior of dissimilar RSW joints and optimize welding parameters for Cu-Al joints. Hence, understanding the joining processes in the electric vehicle industry to design reliable components. Combining different types of materials, such as T2-grade commercially pure copper sheets and aluminum AA1050 with the same thickness of 1 mm has been welded. The determination of optimal welding conditions takes into account material thicknesses and types. Through tensile-shear testing, welding parameters that yield maximal joint strength were identified. Using Minitab 19 software, the Taguchi method helped achieve optimized welding parameters. The hardness, fracture characteristics, and weld strength have been investigated. Hardness measurements were conducted across the nugget thickness and surface, offering insights into potential failure modes. The welding process involves the transition to a liquid state for the aluminum components, resulting in the formation of intermetallic compounds. Consequently, crack initiation was observed within the aluminum segments, leading to a plug-out fracture mechanism. In contrast, copper exhibits superior strength and hardness compared to aluminum, where increased hardness correlates with heightened strength. The discrepancy in hardness, especially the lower values observed on the aluminum side, caused fractures to appear within the heat affected zone (HAZ). Subsequently, this fracture propagated until pull-out failure was realized. The study revealed that dissimilar joining of Cu and Al resulted in an ultimate tensile stress of 26 MPa, while similar joining of copper showcased a strength of 98 MPa. Additionally, the symmetric join in aluminum exhibited a strength of 93 MPa. The maximum tensile shear force is equal to 512 N at a maximum welding current of 14000 A. The pull-out failure mode occurs in the Cu-Al RSW joint. The maximum hardness was noted in the fusion zone (FZ). Relevant literature sources have supported and confirmed these outcomes.

Keywords: aluminium, copper, crack, fracture, hardness, RSW, weld strength

1. INTRODUCTION

Resistance spot welding (RSW) is a process used to join two or more metal sheets or components together. The interface surfaces of most lap configurations are joined by employing an electrical current. RSW stands out as a superior method for fabricating sheet metal due to its simplicity, suitability for various field applications, and flexibility to accommodate the shape of the workpiece (1–6). Many engineering materials that are used in applications are subjected to different mechanical stresses. Therefore, the assessment of crack initiation and prorogation is required to ensure structural integrity (7, 8). Generally, the quality of welded joints determines their structural integrity. Thus, in every manufacturing process, altering the welding procedure and ensuring the quality of the welded joints are crucial (9–12).

The crack of the weld nugget and the structural integrity are the main issues in applications under cyclic loading, such as automobiles and airplanes; see Refs (13–15). The estimation of crack initiation and propagation allows for the evaluation of the fracture analysis. Observing the onset and spread of cracks helps identify flaws early on and ensures the strength of welded joints, which lowers the
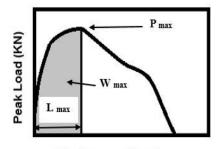
possibility of component failure while in use (16–18).

Copper (Cu) and aluminum (Al) offer superior mechanical qualities, low weight construction, and outstanding thermal and electrical conductivity. Hence, the electric vehicle sector uses them (19).

Because of the significant changes in their metallurgical and physical properties, connecting these materials to the traditional melting welding process is challenging.

Nowadays, lightweight design is in global demand due to energy-saving requirements, enhancing crash safety and strength, and the need to reduce carbon dioxide emissions and fuel consumption (20–24). While the majority of spot welds fail due to fatigue, certain joints might experience failure under tensile loads. Because of the significant changes in their metallurgical and physical properties, connecting these materials to the traditional melting welding process is challenging. A typical load displacement of a spot weld under tensile shear loading is depicted in Fig. 1 (25). Peak load, elongation, and area under the curve (failure energy) can all be used to evaluate the weld strength.

Fig. 1. Load-displacement curve in a tensile test; W_{max}: energy absorption; P_{max}: peak load; L_{max}: elongation at peak load (25)

Since little research has been done on these metals in RSW because of the challenges in fusing copper and aluminium, the majority of earlier studies advised friction stir welding of these dissimilar metals to get around the difficulties in welding between Cu and Al due to their different mechanical and physical properties. This paper's primary goals are to outline the results of mechanical, microstructure, and microhardness tests conducted

both before and after the welding process, as well as to explore the failure mechanism of the RSW of Al-Cu joints under tensile load.

An investigation was conducted on the hardness of the nugget surface and the cross-sectional area.

The Vickers hardness of the weld nugget fusion zone (FZ), heat-affected zone (HAZ), and base material (BM) over the surface and through the cross-section of the weld nugget were measured. The connection between the weld strength and the hardness distribution was investigated. Furthermore, the failure was analysed, and the structural integrity of the spot weld of Al-Cu alloys was shown by the use of the tensile shear test. Therefore, crack initiation and propagation have been estimated.

2. EXPERIMENTAL WORK

2.1. Materials
RSW has been used of dissimilar materials, namely copper T2 grade commercially pure copper sheet and AA1050, with a thickness of 1 mm. They have wide uses in industry, such as electric cars, due to the properties of these materials, the most important of which is electrical conductivity (10,11,26). The chemical composition was examined using a spectrometer to verify the used metals; see Fig. 2.

Fig. 2. Optical Emission Spectrometer

Chemical composition is one of the most important engineering tests carried out by X-ray and optical emission spectroscopy (27). Table 1 shows the results of the chemical composition.
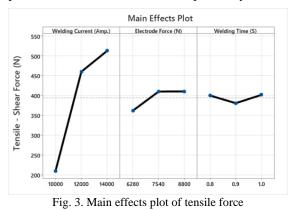
Table 1. Compositions chemical of the materials

Sample %	Si	Fe	Cu	Mn	Mg	Cr	Ni	Zn	Ti	Pb	Sn	V	AL
Al AA1050	0.0477	0.482	0.048	0.0036	0.0012	0.0019	0.0076	0.0027	0.0211	0.0042	0.0098	0.0211	99.5

Sample %	Zn	Pb	P	Mn	Fe	Ni	Si	Mg	AL	Cu	Sample %	Zn	Pb
Cu T2 pure copper sheets	0.003	0.0003	0.0008	0.0004	0.007	0.0002	0.0008	0.0001	0.0029	≈100	Cu T2 pure copper sheets	0.003	0.0003

2.2 Welding Parameters

This work aims to investigate mechanical analysis for resistance spot welding joints. The optimum welding parameters were determined according to the sheet and metal thicknesses. In similar welding materials, we can easily specify the welding parameters, according to the standard AWS C1.1 M/C1 (28). These optimal parameters were determined after welding many samples. Then conducting a practical tensile test, and adopting the sample with the highest tensile strength. The process was made better by applying the Taguchi approach. One of the best techniques for optimizing reduces the trial number by choosing the most efficient parameters and arranging the tests into an orthogonal array (29). Consequently, the welding energy was determined, energy produced depends on the electrical current, time of current flow, and contact resistance (i.e. electrode pressure) (30,31).

The major effects plot illustrates that all of the parameters appear to influence the variation of response (tensile force); see Fig. 3. This method is utilized to examine the impact of each welding parameter on the tensile force independently.

Fig. 3. Main effects plot of tensile force

Finally, the optimum RSW parameters calculate at maximum tensile force (Fig. 3). Table 2 contains a list of the spot-welding parameters that were employed in this study.

Table 2. RSW Parameters

Weld Current (Amp.)	Force (N)	Weld Time (Sec)
14000	8800	1

2.3 Mechanical properties for base metals and RSW joint

2.3.1 Tensile test

The ASTM E-8 standard for thin specimens (ASTM Int. 2009) was followed in the preparation of the specimens of Al and Cu to the stipulated dimensions (32). For each metal, three specimens were tested for more accuracy in results; see Fig. 4.

A universal testing apparatus was used for the tensile testing. A 1 mm/min deformation rate was applied. The maximum load before failure was used to calculate the strength.
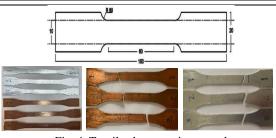

Fig. 4. Tensile-shear specimens and dimensions

2.3.2 Tensile-shear test for RSW joints

Two sheets 100 mm long, 25 mm wide with thickness 1 mm and overlapping 25 mm, have been welded with a single spot weld nugget according to EN ISO 14329 standard (33); see Fig. 5.
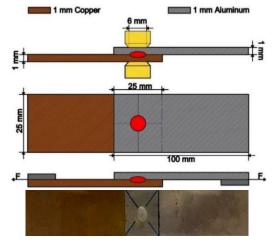

Fig. 5. RSW specimen dimensions

RSW specimens were gripped with alignment tabs of a thickness similar to that of the specimens to ensure the tensile force was applied to the weld spot and to avoid bending (34); see Fig. 6. The tensile shear test findings were made more accurate by repeating the trials and using the average result.
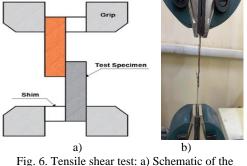

Fig. 6. Tensile shear test: a) Schematic of the specimens with Shims; b) Specimens gripped

Following the tensile shear test, the pull-out failure and fracture propagation were investigated using the macroscopic device; see Fig. 7.
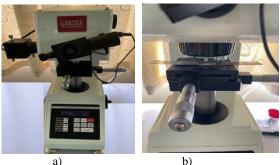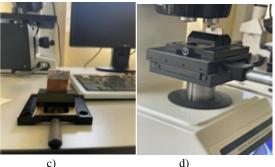
Fig. 7. Macroscopic device

2.3.3 Micro hardness test

In this part, the Vickers microhardness testing device was used, see Figure 8 (a). The size of an impression made under load by a pyramid-shaped diamond indenter is used to determine a material's hardness (35) (36) (37). The micro hardness of the cross-section and top surface were computed; see Fig. 8 (b). The cross-section of RSW joint sample prepared by cutting it transversely and using a special grip to fix the sample; see Fig. 8 (c, d). A 0.98 N applied load and a 15-second dwell period were employed.
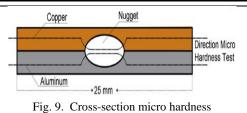

a)   b)

c)   d)

Fig. 8. a) Vickers Micro Hardness Testing device; b) Surface Micro Hardness Measurement for RSW Joint; c) Cross-Section Micro Hardness Specimen with Special Grip; d) Cross-Section Micro hardness measurement

For cross-section micro hardness, the welding sample was cut horizontally and the hardness was measured on two sides Al and Cu; see Fig. 9.

Fig. 9. Cross-section micro hardness

2.3.4 Microstructure test

To conduct the microstructure analysis, the microscope and mounting samples have been used; see Fig. 10.
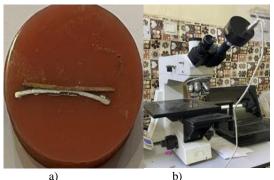

a)   b)

Fig. 10. a) Embedded sample; b) Microscopic device (10)

The specimen for microstructure examination was prepared by following steps:
1. The specimens are small in size; cold compounding was done by hand with acrylic resin (pink and translucent)
2. Grinding the mounted specimen on global polishing and grinding machines using silicon carbide grinding papers of 200, 320, 400, 600, 800, 1000, 1200, and 1500 grains per square inch, respectively.
3. As soon as the grinding phase was finished, the polishing phase got underway. It required using a specific polishing cloth, polishing with an alumina solution (Al_2O_3), spinning the disc at 400 rpm, and then washing it with water.
4. The etching stage started after the polishing stage. Placing the specimen in the etching solution was part of the etching procedure, which was very important to modify according to the concentration. The etching solution in this study is 5g $FeCl_2$, 50 mL HCl, and 100 mL H_2O, (24)
5. Apply the etching for a few seconds; thereafter, in accordance with ASTM E 407-99, specimens were cleaned with water and dried using hot, forced air to avoid surface oxidation (38); see Fig. 10 a.
6. Using a microscope with a digital camera; see Fig. 10 b.

3. RESULTS AND DISCUSSION

3.1 Mechanical properties

The mechanical characteristics, like tensile and yield strengths, for pre-welded metals (Cu and Al) and RSW joints have been founded; see Table 3.

Table 3. Mechanical properties pre-weld metals and RSW joints

Metals	Mechanical Characteristics	
	σ_y (MPa)	UTS (MPa)
Cu-grade T2	135	221
Al-AA1050	119	128
Cu-Al joint	10	26
Cu-Cu joint	37	98
Al-Al joint	39	93

The obtained stress-strain curve for pre-weld Cu and Al and post-weld joints is displayed in Fig. 11.
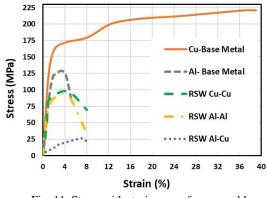

Fig. 11. Stress with strain curve for pre-weld metals and post-weld joints. Al-1050, and pure Cu

Copper has an increased tensile strength in comparison with aluminum because the ductility of copper is greater than that of aluminum and therefore requires greater stress to fail. In RSW joints, the maximum tensile stress for similar weld joints is greater than 75% of the highest tensile strength for dissimilar weld joints; see Fig. 11. Because of the differences in the two welded dissimilar materials' melting temperatures and thermal conductivities, a lower number indicates a weaker junction. Increasing the concentration of heat makes the resulting joint much weaker. In dissimilar welds, two different metals are welded together that have different chemical compositions and mechanical properties (12).

In order to create robust and dependable joints, dissimilar metal welding is a complicated procedure that needs to be carefully considered in many different ways. The challenges associated with mismatched material properties, intermetallic formation, and other factors often lead to reduced maximum tensile strength compared to similar joints. The ultimate tensile strength reached 26 MPa for joining Cu and Al in dissimilar conditions and 98 MPa for joining similar copper, and the symmetric join in aluminum was 93 MPa.
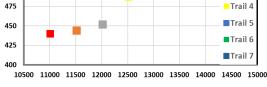
3.2 RSW tensile shear test

Tensile shear testing for RSW joints is the main mechanical test to determine the weld strength. It's the most widely used test due to the simple specimen form and type of loading. It shows if the weld meets the required levels of strength and ductility (12). A universal testing apparatus with a deformation rate of 1 mm/min was used to perform tensile-shear testing. The shear strength force of the welded junction at various welding currents is displayed in Table 4. Because it influences the welding heat input (see Fig. 12), which greatly influences the welding quality and, consequently, the welding duration and electrode force constant, the welding current is the most important process parameter (39).

Table 4. Mechanical properties of a dissimilar RSW joint

Trial	Weld Current (Amp.)	Electrodes Force (N)	Weld Time (sec)	Sheer Force (N)
1	11000	8800	1	440
2	11500	8800	1	444
3	12000	8800	1	452
4	12500	8800	1	487
5	13000	8800	1	492
6	13500	8800	1	499
7	14000	8800	1	512

Fig. 12. Effect of welding current on RSW tensile shear force

The higher welding current increasing tensile shear force. Because a higher welding current generates more heat.

Hence, resulting in better fusion and a stronger bond between the joined materials. As a result, there was an increase in the tensile shear force and bonding strength of the resistance spot-welded connection (40). The maximum tensile shear force is equal to 512 N at maximum welding current 14000 A.

3.3 Failure analysis

Three main forms of failure are frequently observed in spot welds: pullout failure (PF), partial

interfacial (PIF), and interfacial (IF) (31). The crack spreads across the FZ that divides the two sheets in IF mode (41). When a fracture is in PIF mode, it first spreads along the interface before turning perpendicular to the centerline and moving in the direction of thickness. In PF mode, one sheet is removed from the nugget. Hence, the fracture could commence within the BM, HAZ, or HAZ-FZ. In addition, the residual stresses around the weld toe of the nugget play a role (42). The crack around the weld nugget may be subjected to biaxial stresses during propagation; see Ref. (43)

When the internal tensile stresses exceed the strength of the weld joints (i.e., the weld metal, the base metal, or both), the crack has been initiated, and the specimen will be deformed (44). The formation and spread of cracks are also influenced by the residual stress distribution surrounding the weld nugget; see Refs. (42,45). The stress increases significantly once the crack is started, and the crack may spread. One or multiple cracks around the nugget can be propagated simultaneously; see Fig. 13.

Fig. 13. Tensile test for welded joints

Figure 13 shows the crack propagation until the failure. The crack started on the aluminum side and propagated. Different crack propagations have been recorded during the test until the maximum stress.

A crack grows around the nugget in HAZ. Hence, the plug-out fracture was produced. Traditionally, HAZ is a critical zone in the welding area where the properties can be reduced significantly after welding due to cracking (2,31,46). In this zone, the metal is not melted. In addition, the heat changes the metal's microstructure. These changes in structure can reduce the metal's strength (47). Hence, the weld nugget will be withdrawn due to this cracking in the HAZ.

Figure 14 (a-g) shows the fracture in the aluminum nugget zone. The crack was recorded during the time of the tension. In addition, this study indicates that the hardness of the weld nugget gives an indication of the failure behavior. Because the hardness and strength of copper weld nuggets are higher than those of aluminum, the crack was propagated from aluminum only; see Fig. 11.

The macroscopic test shows that PF mode occurs in Cu-Al RSW joint. Initiated of crack from the periphery of the weld nugget on the aluminum side toward the copper side. The HAZ-BM interface on

the aluminum side is where the failure of the welded specimen under static loading began; see Fig. 15. Traditionally, this is associated significantly with the hardness variation.
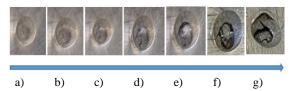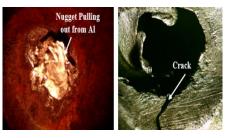

Fig. 14. Initiation with propagation of crack in tensile shear test during consecutive time periods: a) 0 min; b) 1 min; c) 2 min; d) 3 min; e) 4 min; f) 5 min; g) final failure mode
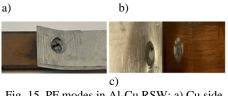

Fig. 15. PF modes in Al-Cu RSW: a) Cu side pull out the Al-nugget side, 10 x; b) Al-nugget side, 10 x; c) Cu and Al nugget after failure

3.4 Micro hardness test

This test aims to show the relationship between hardness and weld strength. In addition, estimate the failure sites. Since hardness is a measure of a material's resistance against scratching or indentation (34,48), it can give an indication of the crack initiation sites.

There are wo types of hardness tests for RSW Cu and Al, namely cross-section microhardness and surface hardness (i.e., over the outer surface of the nugget). Surface hardness measurement was not presented in previous works. This is because the surface hardness in welding of similar metals is clear and equal on both surfaces, but here lies the problem because of the difference in the welded metals, which results in uneven hardness for both surfaces.

3.4.1 Surface hardness

The surface hardness was measured using the device in Fig. 7a. A straight line starts from the first overlap edge toward the other edge overlap for two side RSW joints; see Fig. 7c. The main objective of this test is to indicate the hardness of FZ, BM, and HAZ on the RSW joint surface from two sides.

Different points were taken to check the hardness at different distances along the welded sample. Two sides of the samples were investigated. The first side

represents the copper welding area, Cu nugget, and the second side represents the aluminum welding area, Al nugget; see Fig. 16 (a, b).
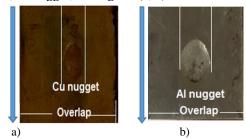

Fig. 16. Welded joints: a) Cu-weld nugget; (b) Al-weld nugget

Table 5. The outer-surface hardness

(Cu) Nugget / Fig. 16 a		(Al) Nugget / Fig. 16 b	
Position mm	Hardness Hv	Position mm	Hardness Hv
0	77.5	0	40
1	80	1	40
2	75	2	42
3	79	3	40
Base Metal Cu — 4	81	Base Metal Al — 4	41
5	82	5	42
6	78	6	40
7	80	7	41
8	80	8	41
HAZ — 9	87	HAZ — 9	48
10	90	10	48
11	91	11	46
Cu Nugget — 13	88	Al Nugget — 13	48
14	87	14	45
15	90	15	48
HAZ — 16	85	HAZ — 16	46
17	78	17	40
18	80	18	41
19	79	19	40
20	79	20	42
Base Metal Cu — 21	81	Base Metal Al — 21	39
22	80	22	41
23	78	23	40
24	78	24	42
25	79	25	40

Table 5 shows the values of the hardness for the two sides of the welded joints, top and bottom; see Fig. 16 a, and b, respectively. In general, the hardness of copper is higher than that of aluminum. Therefore, the fracture from the aluminum weld nugget has been noticed. The maximum hardness at the aluminum and copper weld nugget surfaces is 48 Hv, and 91 Hv, respectively. Then it reduces gradually until it reaches a constant value of the base metals; see Fig. 16. It is mostly dependent on the distribution of temperatures as well as additional factors like the kind and thickness of metals (49,50). The difference in hardness between two sides of the RSW joint means the difference in strength between the two surfaces of the welded joint.
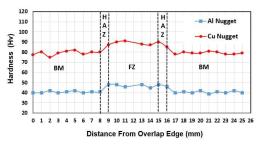

Fig. 17. Surface hardness for RSW joint

3.4.2 Cross-Section micro hardness

For this test, the welding sample was cut horizontally and the hardness was measured on two sides Al and Cu; see Fig. 8.

The weld nugget zone, HAZ, and BM for both spots of the welded sample with ideal welding settings were the three locations for which the Vickers micro hardness measurements were carried out horizontally across the spot welds' cross-section; see Fig. 18. In order to obtain an accurate measurement, the sample was held in a special holder. The measurements were taken at a distance of 1 mm between each point along the cross-section area; see Table 6. The relative decrease in hardness occurs in the HAZ region up to the base metal.

The microhardness of Al 1050 with three different thicknesses (0.6, 1, and 1.5 mm) was investigated in Ref. (51). The comparison with the current study at a thickness of 1 mm is shown in Table 6.
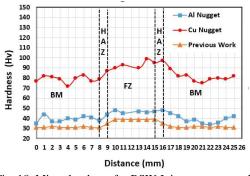

Fig. 18. Micro-hardness for RSW Joints as compared with Ref. (51), thick. = 1 mm

Table 6. Cross-section micro-hardness

(Al) side 1 mm thickness		(Cu) side 1 mm thickness		(Al) (51) 1 mm thickness	
Position mm	Hardness Hv	Position mm	Hardness Hv	Position mm	Hardness Hv
0	35	0	77	0	31
1	44	1	82	1	31
2	37	2	81	2	32
3	37	3	79	3	31
4	40	4	72	4	31
5	39	5	80	5	31
6	42	6	83	6	32
7	41	7	77	7	31
8	38	8	79	8	31
9	44	9	87	9	35
10	48	10	90	10	39
11	45	11	93	11	39
12	47	12	90	12	39
13	46	13	99	13	39
14	47	14	95	14	39
15	48	15	97	15	39
16	45	16	89	16	35
17	42	17	82	17	32
18	37	18	83	18	31
19	39	19	77	19	31
20	35	20	75	20	32
21	34	21	79	21	32
22	36	22	80	22	31
23	40	23	79	23	32
24	42	24	82	24	31
25	39	25	80	25	31

The highest value of hardness was in the center of the nugget. It reached 99 Hv, 48 Hv, 39 Hv for Cu, Al, and Ref. (51), respectively.

Figure 18 shows the through-nugget hardness distribution. The hardness distributions agree with those from the outer surface measurements. In all cases, Cu has a higher hardness than aluminum. In addition, the maximum values of hardness were at the weld nugget. Therefore, the aluminum starts to deform and fracture before the copper weld area. Vickers hardness increased with decreasing grain size and density (52).
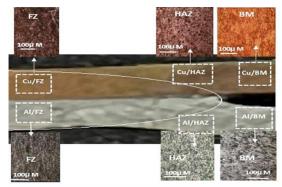

Fig. 19. RSW zones of the Al-Cu Joint

Figure 19 shows the weld zones under a microscopic device. In the cross-section of resistance spot welding joints, three main zones can be observed. The first zone is the Fusion Zone, which represents the area where the base metals have been melted and fused together during the welding process. This region exhibits a distinct microstructure as a result of the solidification of the molten metal. The second zone is the HAZ, surrounding the Fusion Zone, where the base metals have been subjected to high temperatures during welding but have not undergone complete melting. In this zone, there are microstructural changes due to thermal cycles, potentially leading to alterations in material properties. Finally, the third zone is BM, which refers to the unaffected parent material that has not experienced significant thermal or microstructural variations that occur during welding. The received metal is used as a reference point for comparison with the heat-affected zone and fusion zone.

4. CONCLUSIONS

This work studied the strength and hardness of RSW joints made of aluminum (AA1050) and T2-grade commercially pure copper sheets. Tensile testing is commonly used to assess structural integrity. Hardness testing can also provide insight into weld strength. Thus, the weld strength was analyzed by evaluating hardness and crack initiation. The following conclusions were obtained:

1. Taguchi design technique can be used for optimizing RSW parameters for dissimilar joints, which represent the maximum tensile force.
2. Increasing welding current and welding time enhanced nugget size and mechanical strength. However, careful control of these factors is necessary to prevent expulsion in the welding zone.
3. Fracture behavior becomes evident once crack initiation and propagation occur. Tensile tests revealed that pull-out fractures happened more quickly on the aluminum part than on the copper part. Consequently, the weld nugget's strength is higher on the Cu-side.
4. A new relationship between hardness and tensile strength was established to assess failure and strength. Weld nugget portions with higher hardness exhibited greater resistance to cracking, and thus, hardness distribution estimates crack initiation.
5. Surface hardness displayed higher values on the copper side, indicating that pull-out fractures are more likely in the aluminum sheet.
6. During the tensile shear test, crack propagation occurred around the Al-nugget within the HAZ.
7. The highest hardness was at the weld's center. Hardness then decreased towards the HAZ and BM, which exhibited roughly equal hardness values.
8. A microscopic examination of RSW revealed that the BM, HAZ, and FZ had the smallest grain sizes.

Author contributions: *research concept and design, M.S.F., A.A.; Collection and assembly of data, I.A.M.; Data analysis and interpretation, M.S.F., A.A.; Writing the article, M.S.F., A.A.; Critical revision of the article, I.A.M.; Final approval of the article, M.S.F., A.A.*

Declaration of competing interest: *The authors declare that they have no known competing financial interests or personal relationships that could have appeared to influence the work reported in this paper.*

REFERENCES

1. Amin SA, Bakhy SH, Abdullah FB. Study the effect of welding parameters on the residual stresses induced by submerged arc welding process. Journal for Engineering Sciences (NJES) 2017; 20(4): 945–51.
2. Al-Mukhtar AM, Rahman T, Doos QM. Spot welding joint's fracture behavior and fundamental. Fracture, Fatigue and Wear 2019; 18–27. https://doi.org/10.1007/978-981-13-0411-8.
3. Mahmood TR, Doos QM, Al-Mukhtar AM. Failure mechanisms and modeling of spot welded joints in low carbon mild sheets steel and high strength low alloy steel. Procedia Structural Integrity 2018; 9: 71–85. https://doi.org/10.1016/j.prostr.2018.06.013.
4. Al-Mukhtar AM, Al-Jumaili SAK, Al-Jlehawy AHF. Effect of Heat Treatments on 302 Austenitic Stainless Steel Spot Weld. Advanced Engineering Forum 2018; 29:19–25. https://doi.org/10.4028/www.scientific.net/AEF.29.19.
5. Zhang H, Senkara J. Resistance welding: fundamentals and applications. 2011
6. Obaid AY, Mahmood IA, Abood AN. Effects of friction stir processing on microstructural, hardness and damping characteristics of ferritic nodular cast iron. Journal of Engineering Science and Technology 2017; 12(1): 229–40.
7. Abbass M, Ameen H, Hassan K. Effect of heat treatment on corrosion resistance of friction stir welded AA 2024 aluminum alloy. American Journal of Scientific and Industrial Research 2011; 2(2): 297–306. https://doi.org/10.5251/ajsir.2011.2.2.297.306.
8. Fakhri MS, Al-mukhtar A, Mahmood IA. Comparative study of the mechanical properties of spot welded joints. 2022; 1079: 21–8.
9. Radisavljevic I, Zivkovic A, Radovic N, Grabulov V. Influence of FSW parameters on formation quality and mechanical properties of Al 2024-T351 butt welded joints. Transactions of Nonferrous Metals Society of China (English Edition) 2013; 23(12): 3525–39. https://doi.org/10.1016/S1003-6326(13)62897-6.
10. Fakhri M, Mahmood I, Al-Mukhtar A. the electrical and mechanical aspects of aluminum and copper resistance spot weld joints. Engineering and Technology Journal 2023; 0(0): 1–11. https://doi.org/10.30684/etj.2023.143734.1606.
11. Fakhri MS, Al-Mukhtar A, Mahmood IA. Effect of mechanical deformation on the electrical conductivity of resistance spot welding joints. Journal of Applied Science and Engineering (Taiwan) 2024; 27(9): 3095–103. https://doi.org/10.6180/jase.202409_27(9).0007.
12. Khaleel H, Mahmood I, Khoshnaw F. Optimization process of double spots welding of high strength steel using in the automotive industry. Engineering and Technology Journal 2022; 41(1): 110–20. https://doi.org/10.30684/etj.2022.134325.1236.
13. Almukhtar AM. Fracture simulation of welded joints. 2011.
14. Al-Mukhtar AM. Case studies of aircraft fuselage cracking. Advanced Engineering Forum 2019; 33: 11–8. https://doi.org/10.4028/www.scientific.net/AEF.33.11.
15. Al-Mukhtar AM. Aircraft Fuselage Cracking and Simulation. Procedia Structural Integrity 2020; 28: 124–31. https://doi.org/10.1016/j.prostr.2020.10.016.
16. De La Garza M, Zambrano P, Guerrero-Mata MP, Reti T, Réger M, Felde I, et al. Diffusion in electrodes used for resistance spot welding of galvannealed steel. Defect and Diffusion Forum 2010; 297–301: 300–7. https://doi.org/10.4028/www.scientific.net/DDF.297-301.300.
17. Miller Welds. Guidelines for Resistance Spot Welding. Welding Fundamentals and Processes 2018: 10.
18. Tarimer I, Arslan S, Emin Güven M, Karabaş M. A case study of a new spot welding electrode which has the best current density by magnetic analysis solutions. Journal of Electrical Engineering 2011; 62(4): 233–8. https://doi.org/10.2478/v10187-011-0037-8.
19. Sar MH, Ridha MH, Husain IM, Hussein SK. Influence of welding parameters of resistance spot welding on joining aluminum with copper. 2022; 27(2): 217–25. https://doi.org/10.2478/ijame-2022-0029.
20. Manladan SM, Yusof F, Ramesh S, Fadzil M, Luo Z, Ao S. A review on resistance spot welding of aluminum alloys. International Journal of Advanced Manufacturing Technology 2017; 90(1–4): 605–34. https://doi.org/10.1007/s00170-016-9225-9.
21. Hasanbaşoğlu A, Kaçar R. Resistance spot weldability of dissimilar materials (AISI 316L-DIN EN 10130-99 steels). Materials and Design 2007; 28(6): 1794–800. https://doi.org/10.1016/j.matdes.2006.05.013.
22. Ni ZL, Yang JJ, Hao YX, Chen LF, Li S, Wang XX, et al. Ultrasonic spot welding of aluminum to copper: a review. International Journal of Advanced Manufacturing Technology 2020; 107(1–2): 585–606. https://doi.org/10.1007/s00170-020-04997-5.
23. Han L, Thornton M, Boomer D, Shergold M. A correlation study of mechanical strength of resistance spot welding of AA5754 aluminium alloy. Journal of Materials Processing Technology 2011; 211(3): 513–21. https://doi.org/10.1016/j.jmatprotec.2010.11.004.
24. Zare M, Pouranvari M. Metallurgical joining of aluminium and copper using resistance spot welding: microstructure and mechanical properties. Science and Technology of Welding and Joining 2021; 26(6): 461–9. https://doi.org/10.1080/13621718.2021.1935154.
25. Pouranvari M, Marashi SPH. Critical review of automotive steels spot welding: Process, structure and properties. Science and Technology of Welding and Joining 2013; 18(5): 361–403. https://doi.org/10.1179/1362171813Y.0000000120.
26. Wang P, Chen D, Ran Y, Yan Y, Peng H, Jiang X. Fracture characteristics and analysis in dissimilar Cu-Al alloy joints formed via electromagnetic pulse welding. Materials 2019; 12(20). https://doi.org/10.3390/ma12203368.
27. Hassoni SM, Barrak OS, Ismail MI, Hussein SK. Effect of welding parameters of resistance spot welding on mechanical properties and corrosion

resistance of 316L. Materials Research 2022; 25. https://doi.org/10.1590/1980-5373-MR-2021-0117.

28. ANSI/AWS C1. 1M/C1. 1: 2012. Recommended Practices for Resistance Welding.

29. John PWM. Statistical design and analysis of experiments. 1998

30. Al-Mukhtar AM, Doos Q. The spot weldability of carbon steel sheet. Advances in Materials Science and Engineering 2013; 2013: 1–6. https://doi.org/10.1155/2013/146896.

31. Al-Mukhtar AM. Review of Resistance Spot Welding Sheets: Processes and Failure Mode. Advanced Engineering Forum 2016; 17: 31–57. https://doi.org/10.4028/www.scientific.net/AEF.17.31.

32. ASTM E8. ASTM E8/E8M standard test methods for tension testing of metallic materials 1. Annual Book of ASTM Standards 4 2010(C): 1–27. https://doi.org/10.1520/E0008.

33. Standard I, Preview TS. INTERNATIONAL STANDARD of welds — Failure types and geometric iTeh STANDARD PREVIEW iTeh STANDARD PREVIEW. 2003; 2003

34. Barrak OS. Analysis and optimization of resistance spot welding parameters using design of experiment method. 2015.

35. Bakhy S, Amin S, Abdullah F. Influence of SAW Welding Parameters on Microhardness of Steel A516-Gr60. Engineering and Technology Journal 2018; 36(10A): 1039–47. https://doi.org/10.30684/etj.36.10a.4.

36. Shveyov AI, Shveyova TV, Kazantsev RV, Shveyova EI, Shveyev IA. The study of hardness of welded joints of parts in the automotive industry. International Journal of Applied Engineering Research 2017; 12(6): 912.

37. Buranapunviwat K, Sojiphan K. Materials Today : Proceedings Destructive testing and hardness measurement of resistance stud welded joints of ASTM A36 steel. Materials Today: Proceedings 2021. https://doi.org/10.1016/j.matpr.2021.03.562.

38. Practice S. Standard Practice for Microetching Metals and Alloys ASTM E-407. 2016; 07:1–22. https://doi.org/10.1520/E0407-07R15E01.2.

39. Roth S, Hezler A, Pampus O, Coutandin S, Fleischer J. Influence of the process parameter of resistance spot welding and the geometry of weldable load introducing elements for FRP/metal joints on the heat input. Journal of Advanced Joining Processes 2020; 2: 100032.

40. Zhang X, Yao F, Ren Z, Yu H. Effect of welding current on weld formation, microstructure, and mechanical properties in resistance spot welding of CR590T/340Y galvanized dual phase steel. Materials 2018; 11(11): 2310.

41. Tamizi M, Pouranvari M, Movahedi M. The Role of HAZ Softening on Cross-Tension Mechanical Performance of Martensitic Advanced High Strength Steel Resistance Spot Welds. Metallurgical and Materials Transactions A: Physical Metallurgy and Materials Science 2021; 52(2): 655–67. https://doi.org/10.1007/s11661-020-06104-5.

42. Al-Mukhtar AM. Consideration of the residual stress distributions in fatigue crack growth calculations for assessing welded steel joints. Fatigue & Fracture of Engineering Materials & Structures 2013; 36(12): 1352–61. https://doi.org/10.1111/ffe.12060.

43. Al-Mukhtar AM. Mixed-Mode Crack Propagation in Cruciform Joint using Franc2D. Journal of Failure Analysis and Prevention 2016: 1–7. https://doi.org/10.1007/s11668-016-0094-1.

44. Stadler M, Schnitzer R, Gruber M, Steineder K, Hofer C. Microstructure and local mechanical properties of the heat-affected zone of a resistance spot welded medium-mn steel. Materials 2021; 14(12): 3362. https://doi.org/10.3390/ma14123362.

45. Al-Mukhtar AM. Investigation of the thickness effect on the fatigue strength calculation. Journal of failure Analysis and Preventation 2013: 23.

46. Pouranvari M, Marashi SPH, Safanama DS. Failure mode transition in AHSS resistance spot welds. Part II: Experimental investigation and model validation. Materials Science and Engineering: A 2011; 528(29-30): 8344–52. https://doi.org/10.1016/j.msea.2011.08.016.

47. Liu XD, Xu YB, Misra RDK, Peng F, Wang Y, Du YB. Mechanical properties in double pulse resistance spot welding of Q&P 980 steel. Journal of Materials Processing Technology 2019; 263 186–197 p. https://doi.org/10.1016/j.jmatprotec.2018.08.018.

48. Prasad M, Kumar S. Mechanical performance and metallurgical characterization of ultrasonically welded dissimilar joints. Journal of Manufacturing Processes 2017; 25: 443–51. https://doi.org/10.1016/j.jmapro.2017.01.001.

49. Janardhan G, Kishore K, Mukhopadhyay G, Dutta K. Fatigue properties of resistance spot welded dissimilar interstitial-free and high strength micro-alloyed steel sheets. Metals and Materials International 2021; 27(9): 3432–48. https://doi.org/10.1007/s12540-020-00678-w.

50. Boca M, Nagit G, Slătineanu L. Micro hardness in the welded area at resistance spot welding. Advanced Materials Research 2016; 1138: 153–8. https://doi.org/10.4028/www.scientific.net/amr.1138.153.

51. Al Naimi IK, Al Saadi MH, Daws KM, Bay N. Influence of surface pretreatment in resistance spot welding of aluminum AA1050. Production and Manufacturing Research 2015; 3(1): 185–200. https://doi.org/10.1080/21693277.2015.1030795.

52. Lim YY, Chaudhri MM. The influence of grain size on the indentation hardness of high-purity copper and aluminium. Philosophical Magazine A 2002; 82(10): 2071–80.

Marwah Sabah FAKHRI
is a lecturer at the Department of Mechanical Engineering, University of Technology, Iraq. She got her BSc in Mechanical Engineering from the University of Technology, Iraq, in 2007. She then received her M. Sc. in 2016 and her PhD in Engineering/Applied Mechanical from the University of Technology in 2024.
Her research interests encompass the mechanical behaviour of materials, cracks, failure analysis, fracture simulation, and materials testing.
e-mail: me.20.24@grad.uotechnology.edu.iq

Fakhri M, Al-Mukhtar A, Mahmood A: *Mechanical behaviour and failure mechanism of resistance spot …*

Dr. Al-Mukhtar received his Ph.D. in Materials Engineering from TUBA Freiberg, Germany, in 2010. He conducted post-doctoral work from 2010 to 2015 on the fracture behaviour of materials at TUBAF, Germany. Recently, he affiliated as an external Postdoctoral Researcher at Bauhaus-Universität Weimar in Germany. He earned his MSc and BSc from Baghdad University, College of Engineering, Mechanical and Aeronautical Engineering Department in Iraq.

He has held various positions at universities in different countries, primarily as an assistant professor. His research interests encompass the mechanical behaviour of materials, cracks, failure analysis, fracture simulation, and materials testing (Materialprüfung).

e-mail: almukhtar@structuralintegrity.eu

Ibtihal A. MAHMOOD received her Ph.D. (2004) in production engineering and metallurgy from University of Technology- Iraq. She graduated from University of Technology - Iraq for her bachelor and master degrees. Currently, she is a faculty member in the Department of Mechanical Engineering, University of Technology- Iraq.

She authored and co-authored more than 45 papers some of papers published in high ranking prestigious international journals and conferences. With co-authors she has authored three textbooks that are currently taught in (Vocational Education Schools). Supervising more than 27 master's and doctoral students and more than 35 university project students.

2007-2008 Visiting professor in- Al-Balka University Engineering Department–in Jordon at 2007.

2017-2018 Visiting professor in- Plymouth University- mechanical engineering Department–in UK at 2017.

e-mail: 20183@uotechnology.edu.iq